ELSEVIER

Contents lists available at ScienceDirect

Science of the Total Environment

journal homepage: www.elsevier.com/locate/scitotenv





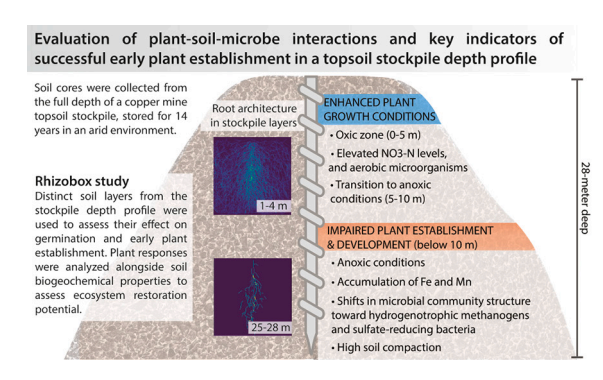
Depth-dependent heterogeneity in topsoil stockpiles influences plant-microbe interactions and revegetation success in arid mine reclamation

Kamila Murawska-Wlodarczyk^{a,*}, Priyanka Kushwaha^a, Owyn Stokes^a, Craig Rasmussen^a, Julia W. Neilson^a, Raina M. Maier^a, Alicja Babst-Kostecka^{a,b}

HIGHLIGHTS

- Topsoil stockpiles exhibit strong biogeochemical heterogeneity across depths.
- Stockpile microbiome shifts are associated with vegetation establishment.
- Germination and plant growth are influenced by distinct soil variables.
- Anaerobic conditions in deeper layers are linked to reduced plant establishment.
- Plant-soil feedbacks may contribute to fungal recovery in degraded stockpile soils.

GRAPHICAL ABSTRACT



MAIN FINDINGS

- High biogeochemical heterogeneity exists across depths, resulting in a patchy distribution of soil quality within the stockpile.
- Soil microbial communities and their functions, in combination with soil chemistry, play a key role in germination and plant establishment across varying stockpile layers.
- Plant-soil feedback mechanisms drive soil recovery, including fungal community renewal, as evidenced by changes in soil parameters before and after the
- Stockpile formation processess strongly influence soil health and future ecosystem recovery potential.

ARTICLE INFO

Keywords:
Plant-soil-microbial interaction
Soil recovery
Soil microbiome
Post-mining reclamation
Soil health
Semi-arid ecosystem
Tonsoil stockpile

ABSTRACT

Covering mine tailings with uncontaminated soil is a common strategy to mitigate environmental impacts and promote ecosystem recovery during post-mining land reclamation. Topsoil is often stockpiled for future use as a capping layer, but prolonged storage alters its physical, chemical, and microbial properties, often hindering revegetation.

This study evaluated soil health parameters within the 28-meter depth profile of a 14-year-old copper mine topsoil stockpile to identify key indicators of revegetation success in semi-arid ecosystem. Using non-invasive root phenotyping in rhizoboxes, filled with soils collected from different depth layers, we monitored plant growth and assessed how biochemical variability in stockpile materials affects germination and early establishment. Machine learning models integrating soil properties, plant responses, and sequenced soil bacterial/archaeal and fungal DNA, identified key indicators influencing plant performance.

Results revealed significant heterogeneity in soil quality across depths, with distinct biochemical and microbial profiles shaping vegetation establishment. The upper 10 m exhibited greater potential for supporting growth, with seedling survival reaching 95 %, whereas deeper layers showed drastically reduced survival, sometimes as low as 0 %, due to microbial shifts to anoxic conditions and elevated Fe and Mn toxicity. Fungal

E-mail address: kamilamurawska@arizona.edu (K. Murawska-Wlodarczyk).

^a Department of Environmental Science, The University of Arizona, Tucson, 85719, AZ, USA

b BIO5 Institute, The University of Arizona, Tucson, 85719, AZ, USA

^{*} Corresponding author.

communities played a dominant role in germination, while archaea were more influential during later plant establishment. Soil parameter comparisons before and after the experiment indicated recovery processes initiated by plant-soil feedback, including fungal community renewal. These findings highlight the role of stockpile formation in preserving soil health attributes critical for ecological recovery and provide practical insights for optimizing land reclamation in semi-arid ecosystems.

1. Introduction

The global demand for natural resources has surged, intensifying mining activities and driving economic and industrial growth. Yet, this progress comes at a high environmental cost. Mining operations alter landscapes, stripping vegetation, depleting topsoil, and destroying habitats, often leading to severe biodiversity loss and ecosystem degradation (Li et al., 2022). The environmental impacts extend beyond the mining sites, triggering soil erosion, groundwater pollution, and lowered air quality in surrounding areas. These ecological changes are closely intertwined with social implications, disproportionately affecting nearby communities by compromising environmental health, limiting access to natural resources, and exacerbating environmental injustices (Aleksandrova and Timofeeva, 2021).

To mitigate these impacts, mining companies are required to rehabilitate disturbed lands post-closure. These efforts aim to create stable, non-polluting landscapes that can support self-sustaining vegetation and promote ecosystem recovery (Manero et al., 2020). However, current regulations often lack detailed guidance for achieving long-term ecological restoration. Many reclamation efforts rely on cost-effective methods or outdated approaches, which may not align with the ecological principles of natural succession, leading to high-risk and unsustainable outcomes.

Topsoil stockpiling is a common practice in post-mining land reclamation, aimed at preserving nutrient-rich soil layers for future reclamation use (Cooke and Johnson, 2002). Despite its utility, the processes of excavating, storing, and reapplying topsoil have impacts that can compromise reclamation success. Research progressively uncovers the adverse effects of stockpile height and storage duration on soil health, but also highlights a strong depth-dependent variation in soil quality (Fischer et al., 2022; Mushia et al., 2016). Prolonged storage induces physical and biogeochemical changes, reducing soil's capacity for ecosystem recovery. Major alterations include decreased aggregate stability, increased compaction, lower nutrient availability, and declines in organic carbon content and water-holding capacity. Changes in pH and oxygen depletion with depth further exacerbate soil degradation over time (Abdul-Kareem and McRea, 1984; Harris et al., 1993). These changes negatively impact microbial communities, crucial for nutrient cycling and soil health (D'Agui et al., 2022; Hernandez et al., 2024), further complicating plant establishment in reclaimed soils.

Reclamation outcomes largely depend on soil health and functionality, which are inherently site-specific and shaped by a complex interplay of biogeochemical variables (D'Agui et al., 2022). This is particularly challenging in arid and semi-arid ecosystems, where harsh ecological conditions - characterized by poor soil quality, low water content, and other limiting factors - frequently result in failed vegetation establishment during reclamation efforts (Shackelford et al., 2021). Most studies on topsoil stockpiling have been conducted in temperate climates and have focused on shallow stockpile depths (typically up to 5 m), which may not fully capture the conditions of hard-rock mining sites, where stockpiles are much larger, stored for longer periods, and often exhibit stronger vertical gradients in soil quality (Amir et al., 2022; Fischer et al., 2022; Mushia et al., 2016). This leaves a critical knowledge gap in understanding plant-soil interactions in deeper layers, where prolonged storage may impair soil structure, geochemistry, and microbial functioning, ultimately affecting plant establishment particularly under extreme climatic and environmental conditions in post-mining reclamation projects (Amir et al., 2022).

This study assessed specific soil health parameters along the 28 m depth profile of a 14-year-old copper mine topsoil stockpile in a semiarid ecosystem - a depth rarely examined in previous studies - to evaluate the suitability of the stockpiled soil for revegetation when used in future reclamation. Previous biogeochemical analysis revealed significant heterogeneity along the stockpile depth profile, likely driven by buried plant material and oxygen limitations at deeper layers, resulting in anaerobic conditions (Ledesma et al., 2025). Stockpiling can also lead to the accumulation of potentially toxic forms of Fe and Mn, thereby suppressing the growth of plant-growth-promoting bacteria, altering microbial community composition, and reducing nutrient availability (Weber et al., 2006). As the implications of this variability for reclamation remain unclear, this study evaluates the consequences for soil health, microbial functioning, and plant establishment. We hypothesize that the observed heterogeneity alters microbial community structure and biogeochemical cycling, leading to depth-dependent shifts in nutrient and toxin accumulation, and ultimately to compromised plant responses, particularly when grown on material from deeper, potentially anoxic layers. Specifically, we expect deeper layers to exhibit stronger nutrient limitations, greater accumulation of phytotoxic compounds, and a shift toward more anaerobic microbial communities compared to surface soils. To test this, we used a rhizobox system that allowed controlled comparisons of plant responses to soil layers from different depths of the stockpile. Using this non-invasive root phenotyping technique, we monitored the growth of Atriplex lentiformis, a perennial halophyte native to the semi-arid regions of southwestern USA, across soil layers collected from different stockpile depths to assess how soil depth influences early plant establishment. While rooting at such extreme depths is unlikely under natural conditions, our study was designed in collaboration with the mining industry and reflects realworld constraints of large-scale reclamation. In practice, the entire volume of stockpiled topsoil – regardless of depth – is often used due to limited availability of capping material. Consequently, plant roots are likely to encounter soil from across the full depth profile during reclamation. Specific questions we ask include: (1) What biogeochemical changes occur along the stockpile depth profile, that may influence soil health and reclamation potential? (2) Which specific stockpile soil factors affect germination and plant establishment? (3) Do stockpile soil material recover following water addition and plant establishment? The results presented enhance understanding of soil quality variability and plant-soil-microbe interactions within stockpile materials, providing valuable insights to inform effective reclamation strategies in arid and semi-arid ecosystems.

2. Materials and methods

2.1. Study area, and sampling of soil and plant materials

Soil samples were collected in April 2021 from a 14-year-old topsoil stockpile at a copper mine near Globe, Arizona, USA. The region has a semi-arid climate with an average annual rainfall of 50 cm and mean annual temperature of 20 °C. A drill rig was set up to core two boreholes, each with a diameter of 10 cm, located $\sim\!25$ m apart, and each drilled until the underlying bedrock layer: Core 1 (15 m deep) and Core 2 (28 m deep) (Fig. 1). The variation in core depths corresponds to differences in the surface geology along the slope where the topsoil was deposited. Each core was divided into sub-layers, identified through visual assessment of soil properties (color and texture) at varying depths. Areas

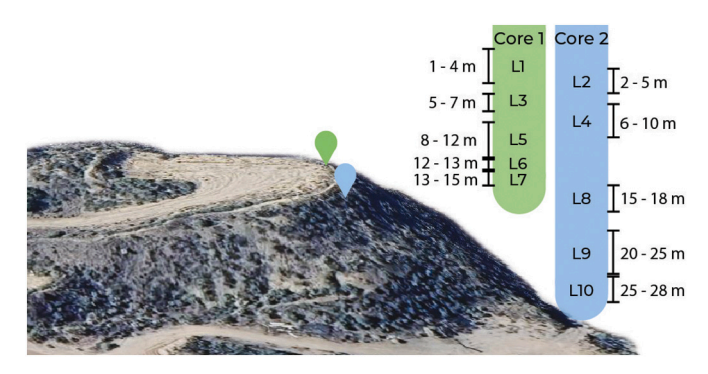


Fig. 1. Sampling location and soil layers. A 3D view of sampling location, with details on the depths of the cored bore holes and the soil layers used in the phenotyping experiment. Imagery of the topsoil stockpile near Globe, Arizona, USA, obtained from Google Earth (accessed on 08/14/2023).

with larger rocks and pebbles were excluded (Supplementary material), and the remaining material included in this study was labeled by physical depth of distinct soil layers across both cores, representing 10 depth layers as shown in Fig. 1. Soils from both cores were categorized as sandy loam, with 25–43 % silt and clay, and up to 75 % sand (Ledesma et al., 2025). Soil from each layer was sieved through a 4 mm mesh to preserve soil aggregates and then homogenized. From each depth layer, three independent soil subsamples(150 g; 10 layers \times 3) were collected for chemical analysis (air-dried and stored at room temperature) and additional triplicate 2 g samples were collected for microbial analysis (collected using sterile tools, placed into sterile tubes, and stored at $-80\,^{\circ}\mathrm{C}$ until further processing). These samples are further referred to as "Start soils" (i.e., prior to the rhizobox experiment).

Atriplex lentiformis seeds were collected from two distinct locations in Arizona, USA. This species is a drought-tolerant shrub native to the southwestern USA, commonly used in arid land reclamation due to its resilience, metal tolerance, and ability to establish in disturbed soils (Mendez et al., 2007; Murawska-Wlodarczyk et al., 2024). The two accessions were selected to test whether contrasting edaphic conditions (non-metalliferous vs. metalliferous soils) confer differences in plant adaptation traits, which could influence accession-specific performance in reclamation settings. The non-metalliferous site (NM), denoted as NM-PHX, was located within the Rio Salado Audubon Center nature reserve in Phoenix (33°25'09.7"N 112°04'20.9"W). The metalliferous (M) site, referred as M-IK, was located ~150 km north of Phoenix, within the Iron King (IK) Mine and Humboldt Smelter tailings site in town of Dewey-Humboldt (34°50'07.32"N 112°25'25.12"W). Ripe seeds (> 100 per plant) were collected from five A. lentiformis plants at each site, combined into a bulk sample for each location, and stored at room temperature. Given the hard seed bracts of A. lentiformis, seeds were soaked in deionized water under dark conditions at 4 °C for 7 days prior to the experiment to trigger metabolic processes necessary for germination and to reduce variability in germination timing.

2.2. Phenotypic variability in A. lentiformis in response to different layers of the stockpiled material: experiment in rhizoboxes

Equal volumes (200 mL) of sieved, homogenized soil were added to rhizoboxes ($12 \times 12 \times 1.5$ cm) to ensure consistent bulk density across treatments. Each soil sample was individually moistened with deionized water to achieve comparable soil moisture levels across treatments. Ten replicates per soil layer were prepared for each of the two *A. lentiformis* accessions, along with two control rhizoboxes without plants. Due to limited soil material, layers L6, L8, L9, and L10 had five replicates and one control. In total, the experimental design comprised 176 rhizoboxes. Seeds of both accessions were randomly selected, individually placed in rhizoboxes, and covered with a thin layer (\sim 3 mm) of soil. The rhizoboxes were positioned at a 45° angle to facilitate root system

observation along the inner surface and were separated by polyethylene foam to provide thermal insulation and protect the roots from light exposure. The study was conducted under controlled conditions with a 12 h light/dark cycle, light intensity of 100 $\mu mol\cdot m^{-2}\cdot s^{-1}$, and day/night temperatures of 20°/17 °C. The rhizoboxes were irrigated daily with deionized water, and their locations on the growth platform were randomly rearranged every seven days.

Seed germination and seedling survival were monitored daily, to assess the effects of soil material quality and plant accession on germination success and seedling mortality. Each rhizobox contained only one seed at a time. To maximize the number of plants cultivated in the rhizoboxes, seeds that did not germinate within 14 days of seeding were classified as 'non-germinated', removed, and replaced with new seeds. This time frame was based on previous studies indicating an average germination time of 12 days for this species (Murawska-Wlodarczyk et al., 2024). New seeds were also added in cases of seedling death. Seed replacement was discontinued six weeks after the start of the experiment, allowing for a total of three seed replacements. Seedling survival and mortality were calculated as the percentage of germinated seeds that survived or died by the end of the experiment, respectively, relative to the total number of seeds that germinated. The germination percentage (germination %) and the percentage of non-germinated seeds were calculated as the proportion of seeds that germinated, and the proportion of seeds that failed to germinate within 14 days, respectively, both relative to the total number of seeds added to the rhizoboxes, including replacements.

Non-invasive measurements of below- and above-ground plant parameters were conducted at 7-day intervals, starting seven days after seed germination, for a total of 9 measurements. The development of the root system was monitored by manually tracing the roots visible on the inner surface of the rhizobox onto a transparent plastic foil. ImageJ software was employed to analyze root drawings and to assess temporal changes in the total root length (Schneider et al., 2012). Plant height and leaf number were recorded, and high-resolution images (6000×4000 pixels, 350 dpi, Sony A6400, Tokyo, Japan) were taken for leaf area (cm²) assessment (Easy Leaf Area software) (Easlon and Bloom, 2014).

At harvest, 9-weeks after germination, final measurements of plant parameters were taken along with a visual assessment of plant health and stress symptoms (chlorosis and necrosis) and the fresh aboveground biomass weight (g). Rhizosphere-influenced soil (\sim 7 g) was collected from the immediate vicinity of the roots using sterile spatulas, placed into sterile tubes, and promptly stored at $-80\,^{\circ}$ C until further processing. The remaining soil material from each rhizobox was stored at room temperature for subsequent chemical analysis.

2.3. Chemical analyses of soil and plant samples

Soil samples were air dried for 72 h, sieved with a 2-mm mesh, and sent to an external laboratory for analysis of: pH (1:1 (w/v) suspension of soil in ultrapure water), organic matter (OM), nitrate nitrogen (NO $_3$ -N), ammonium nitrogen (NH $_4$ -N), water extractable organic carbon (CWEOC), water extractable organic nitrogen (Norg), Olsen phosphorus (Polsen), ammonium acetate extractable sulfur (S), calcium (Ca), magnesium (Mg), potassium (K), sodium (Na), and DTPA extractable fraction of: iron (Fe), manganese (Mn), copper (Cu), and zinc (Zn). Analytical methods follow Brookside Labs' standard soil testing protocols (https://www.blinc.com/soil-testing-methods).

Due to low plant biomass, the aboveground plant parts (stems and leaves) were pooled into one composite sample per soil treatment, representing the respective stockpile depth layer. Samples were ovendried at 70 °C for 72 h, cooled in a vacuum desiccator, packed into 4.5 mL tubes with ceramic spheres (TallPrep Lysing Matrix M, 4.5 mL tube; MP Biomedicals), and finely ground to a homogenous powder using a FastPrep-24 5G homogenizer (MP Biomedicals). Ground plant material (0.1 g) was pre-digested with 1 mL concentrated HNO₃ (Ari-Star Plus HNO₃, BDH Chemicals) at room temperature for 4 h, followed

by the addition of 1 mL $\rm H_2O_2$ (30 % Suprapure $\rm H_2O_2$, EMD). After the $\rm H_2O_2$ reaction subsided, 1 mL of ultrapure water (18 Ω) was added, the vessels were capped, and samples were subjected to microwave digestion (CEM Model MARS 6, Matthews, North Carolina). The digestion program used for plant samples is a slow ramp over 20–25 min to 200 °C, followed by 10 min at 200 °C. Controls included an acid blank and a certified reference material (NIST #1515 Apple Leaves). Bulk elemental analysis was performed on all samples using ICP-MS (Agilent 7700x, Santa Clara, CA) for Na, Mg, P, S, K, Ca, Mn, Fe, Cu, and Zn. Sample digestion and ICP-MS analysis were conducted by the Arizona Laboratory for Emerging Contaminants (ALEC) at the University of Arizona, Tucson, AZ.

2.4. Soil microbiome DNA extraction, sequencing, and bioinformatics

DNA was extracted from ~ 0.25 g of soil using the QIAGEN DNeasy PowerLyzer PowerSoil kit, following the manufacturer's instructions. Negative control samples (blanks) consisting only of reagents were included throughout the process. The DNA was quantified using a Qubit 4.0 Fluorometer and a high sensitivity dsDNA assay (Invitrogen, Carlsbad, California, USA). Soil DNA biomass (ng g $^{-1}$ of dry soil) was calculated based on the soil moisture content of each sample.

To analyze bacterial/archaeal and fungal communities, the V4 region of the 16S ribosomal RNA (rRNA) gene was amplified using the 515F/806R primers, and the fungal internal transcribed spacer (ITS) region was amplified using the ITS1f-ITS2 primers (Walters et al., 2016). The purified amplicons from all samples were pooled in equimolar concentrations and subjected to paired-end sequencing (2×150 bp) on the Illumina MiSeq platform (Illumina, Inc., CA, USA) at the University of Arizona's Microbiome Core. Bioinformatics analyses were carried out using the DADA2 pipeline (Callahan et al., 2016) as detailed in the Supplementary material. The functional potential of the bacteria/archaea and fungi was predicted from 16S rRNA and ITS taxonomic assignments using the FAPROTAX and FUNGuild databases, respectively (Louca et al., 2016; Nguyen et al., 2016). The raw sequencing data for bacteria/archaea and fungi can be accessed in NCBI's Sequence Read Archive under BioProject PRJNA1180669.

2.5. Statistical analyses

The soil samples were divided into three categories: i) Start soil representing properties of soils before the experiment in rhizoboxes, ii) Plant-affected soil - collected at harvest, i.e., after 9-weeks of plant growth in the rhizobox, and iii) Control soil - collected at harvest from control (without plants) rhizoboxes. The soil and plant data were checked for normality using the Shapiro-Wilk test and for the homogeneity of variance using Levene's test. Normalization functions from the bestNormalize package in R (Peterson and Cavanaugh, 2019) were applied to variables that did not meet the assumptions for parametric tests (Shapiro-Wilk test, p < 0.05). While the majority of soil parameters were normalized after transformation and subsequently analyzed using parametric one-way ANOVA, non-parametric Kruskal-Wallis test was used for Mn, Zn, NO₃-N, C_{WEOC}, N_{org}, and soil DNA biomass, as these parameters did not meet the necessary assumptions. Tukey's HSD and Dunn's multiple comparisons post-hoc tests were conducted following ANOVA and Kruskal-Wallis test, respectively, to further investigate the significant differences.

Differences in plant parameters (root length, leaf area, leaf number, and height) at harvest were assessed using the Kruskal-Wallis test with Bonferroni correction, followed by Dunn pos-hoc test. Differences in mean root length across soil layers were tested at each of the 9 measurement points (*Time*) using the same approach. To evaluate the significant differences in root growth within each soil layer over *Time*, repeated measures ANOVA was applied, followed by pairwise *t*-tests with Bonferroni correction. The effect of *Population* on the pace of root growth was assessed using nested ANOVA, with *Time* as the main factor

and Population nested within Time.

Alpha diversity metrics, including richness and Shannon index, along with beta diversity of the microbial community, were computed utilizing the vegan package (Oksanen et al., 2008). Community dissimilarity was quantified using the Bray-Curtis distance metric. To visualize the differences in microbial community composition, non-metric multidimensional scaling (NMDS) ordination plots were generated. The effect of soil layer and category as well as the core on community composition differences were determined using nested permutational multivariate analysis of variance (PERMANOVA). Significant microbial taxa were identified using a Kruskal-Wallis test, adjusted for multiple comparisons, and filtered for taxa with relative abundances >1 % and adjusted pvalues < 0.05. These organisms (identified separately for Start and Plantaffected soils) were then used in the Partial Least Square (PLS) regression. Distinct taxa were identified as those with relative abundance values exceeding half of the maximum observed value and present in only one layer.

The variation in germination and plant performance metrics across different soil layers was analyzed using PLS regression models (see the Supplementary Methods for details on PLS methodology). Differences in soil parameters, relative abundance of microbial taxa, and microbial functional predictions across soil categories (*Start - Control - Plantaffected*) for each soil layer were assessed with Kruskal-Wallis test. Note that the main figures and tables represent data merged at the species level (*A. lentiformis*), while differences between the populations (if significant) are represented in the Supplementary material.

All analyses were performed in R 4.3.0 (R Core Team, Vienna, Austria) except for PLS, that was conducted using XLSTAT Statistical Software for Excel (Addinsoft, New York, USA).

3. Results

3.1. Biogeochemical characteristics of the soil layers prior to the phenotyping experiment

Significant differences were observed across all parameters in the Start soils (Table 1). The pH ranged from 6.7 to 8.4, indicating neutral to alkaline conditions, with no clear depth-related trends. The OM% was slightly over 1 % in most of the soils, except three layers (< 1 %): L1₍₁₋ _{4m)}, L4_(6-10m), and L8_(15-18m). Concentrations of macronutrients such as Ca and Mg ranged from 1400 to 3860 mg kg $^{-1}$ and 210 to 490 mg kg $^{-1}$ respectively. Sodium levels ranged from 30 to 60 mg kg⁻¹, with peaks of 110 mg kg^{-1} in $L4_{(6-10\text{m})}$, and 89 mg kg^{-1} in $L8_{(15-18\text{m})}$. The uppermost layers of both cores (1-5 m) had the highest concentrations of Polsen, NO₃-N, N_{org}, and C_{WEOC}, which dropped significantly in all the lower layers (except for P_{Olsen} in L10_(25-28m), and N_{org} for L6_(12-13m) and L10_(25-28m) _{28m}). In contrast, NH₄-N concentrations increased in the deeper parts of the stockpile (except L4_(6-10m) and L8_(15-18m)), highlighting the variability of nitrogen forms throughout the stockpile profile. Similarly, Fe (except L8_(15-18m)) and Mn concentrations tended to increase with depth. Potassium ($< 160 \text{ mg kg}^{-1}$) and Zn ($< 3.5 \text{ mg kg}^{-1}$) remained low across all the layers. Copper ranged from 2.5 to 29 mg kg⁻¹ in most soils, except 43 mg \mbox{kg}^{-1} in L3 $_{(5\mbox{-}7m)}$. Sulfur concentrations were within typical ranges for arid soils (10–100 mg kg⁻¹), except for significant enrichment of $\sim 700 \text{ mg kg}^{-1}$ in L8_(15-18m).

The microbial DNA biomass ranged from 28 to 1470 ng g $^{-1}$, with the lowest values observed at depths of 5 to 10 m. Bacterial/archaeal and fungal richness varied from 459 to 934 and from 14 to 56, respectively. Shannon diversity indices spanned from 3.5 to 5.7 for bacteria/archaea and 1.7 to 3.3 for fungal communities. Across these measures, no consistent trend related to depth was observed.

3.2. Microbial community composition and functional predictions in "Start soil"

NMDS analysis of the Start soils showed significant distinctions in

Table 1
Biochemical characteristics (mean \pm SE, n=3) of the stockpile soil layers prior to the rhizobox experiment (*Start soils*). Concentrations of soluble S; P_{Olsen}; total concentration of: Ca, Mg, K, Na; DTPA extractable fractions of: Fe, Mn, Cu, Zn; NO₃-N, NH₄-N, water extractable organic carbon (C_{WEOC}) and nitrogen (N_{org}) are expressed in mg kg⁻¹. OM - organic matter. Different letters indicate statistically significant differences at $p \le 0.05$.

Soil layer	L1	L2	L3	L4	L5	L6	L7	L8	L9	L10
Layer depth (m)	1–4	2–5	5–7	6–10	8–12	12–13	13–15	15–18	20–25	25–28
pH	7.9 ±	7.9 ±	$7.2\pm0.03^{\rm f}$	8.4 \pm	6.7 ± 0.1^{g}	$8.1\pm0.03^{\rm b}$	$7.5\pm0.1^{\rm d}$	$7.7\pm0.08^{\rm c}$	7.2 ±	7.4 ±
	0.06^{bc}	0.03 ^{bc}	,	0.05^{a}	,		,		$0.01^{\rm ef}$	0.01^{de}
OM %	0.93 ±	1.2 ±	$1.3\pm0.03^{\rm b}$	0.55 ±	$1.2\pm0.03^{\mathrm{bc}}$	$1.1\pm0^{\mathrm{c}}$	1.2 ± 0^{bc}	$0.6\pm0.04^{\text{e}}$	1.3 ±	1.8 ±
	0.03 ^d	0.03 ^{bc}		0.05 ^e	=o · ord	de	a== , ,de	co=	0.05 ^b	0.07 ^a
S	$29 \pm 2^{ef} \ 9.7 \pm 0.3^{ab}$	$76 \pm 2^{ m bc} \ 7.3 \pm 0.7^{ m bc}$	104 ± 7^{b} 5 + 0.6 ^{bcd}	$\begin{matrix}22\pm0^{\mathrm{f}}\\2+0^{\mathrm{d}}\end{matrix}$	$52 \pm 3^{cd} \ 4.7 \pm 2^{cd}$	$\begin{array}{l} 40\pm1^{de} \\ 6.3\pm1.2^{bcd} \end{array}$	$37.5 \pm 4^{de} \ 4.5 \pm 2.5^{cd}$	697 ± 2^{a} $2 + 0^{d}$	71 ± 1^{c} 5 ± 1^{bcd}	$\begin{array}{c} 11\pm1^{\mathrm{g}} \\ 13\pm0.9^{\mathrm{a}} \end{array}$
P _{Olsen}	$9.7 \pm 0.3^{\circ}$ $3183 \pm 22^{\circ}$	7.3 ± 0.7 3861 ± 33^{a}	5 ± 0.6 1736 ±	2 ± 0 2621 ±	4.7 ± 2^{h} 1452 ± 20^{h}	6.3 ± 1.2 2626 ± 37^{d}	4.5 ± 2.5 1637 ± 17^{g}	2 ± 0 3396 ± 8 ^b	5 ± 1 1830 ± 6^{f}	13 ± 0.9 2211 ±
Ca	3183 ± 22	3801 ± 33	1/36 ± 51 ^{fg}	43 ^d	1452 ± 20	2020 ± 37	1637 ± 17°	3390 ± 8	1830 ± 0	2211 ± 12 ^e
Mg	$216\pm3^{\text{g}}$	247 ± 5^{ef}	305 ± 9^{cd}	209 ± 1.5^{h}	295 ± 3^{cde}	227 ± 4^{fg}	280 ± 4^{def}	$\begin{array}{l} 329 \pm \\ 0.8^{bc} \end{array}$	366 ± 2^{b}	490 ± 6^a
Ca:Mg	$\begin{array}{c} \textbf{14.7} \pm\\ \textbf{0.1}^{\text{b}} \end{array}$	$15.6\pm0.3^{\text{a}}$	$5.7\pm0.1^{\rm f}$	$12.6 \pm \\0.1^{c}$	4.9 ± 0.1^{gh}	11.6 ± 0.1^{d}	$5.8 \pm 0.1^{\rm f}$	$10.3 \pm 0.1^{\text{e}}$	$\textbf{5.0} \pm \textbf{0.1}^{g}$	4.5 ± 0.1^{h}
K	84 ± 4^{cd}	64 ± 1^{ef}	91 ± 2^{bcd}	$61\pm2^{\rm f}$	65 ± 3^{ef}	132 ± 2^{ab}	76 ± 1^{de}	99 ± 1^{bc}	90 ± 2^{cd}	154 ± 2^a
Na	$46\pm0.6^{\rm f}$	$49\pm0.6^{\rm f}$	58 ± 2^{cd}	110 ± 2^a	$30\pm0.6^{\rm g}$	55 ± 1^{de}	$51\pm1^{ m ef}$	$89\pm1^{\rm b}$	58 ± 2^{cd}	61 ± 1^{c}
Fe	$7.3\pm0.3^{\rm f}$	$\begin{array}{c} 13.7 \pm \\ 0.9^{\text{def}} \end{array}$	$\begin{array}{l} 42.7 \pm \\ 1.8^{bc} \end{array}$	$2.5\pm0.5^{\text{g}}$	63 ± 6^a	$\begin{array}{l} \textbf{32.7} \pm\\ \textbf{3.2}^{\text{cde}} \end{array}$	43 ± 3^{bc}	9 ± 0.8^{ef}	54 ± 0.6^{b}	39 ± 1.5^{cd}
Mn	$\begin{array}{l} 8.3 \pm \\ 0.3^{\rm abc} \end{array}$	3.7 ± 1.2^{c}	$32.3 \pm \\3.5^{abc}$	3.5 ± 0.5^{bc}	$\begin{array}{c} 20.7 \pm \\ 17.2^{abc} \end{array}$	$\begin{array}{l} \textbf{23.3} \pm \\ \textbf{2.9}^{abc} \end{array}$	17 ± 2^{abc}	41 ± 0.8^{abc}	96 ± 1^{ab}	122 ± 0.6^a
Cu	9.9 ± 0.1^{ef}	$15.1 \pm \\1.2^{\rm cde}$	43.1 ± 1.9^a	2.5 ± 0.1^e	$\begin{array}{c} 23.9 \pm \\ 1.7^{bcd} \end{array}$	15 ± 0.7^{cde}	$14.8 \pm \\1.0^{\rm cde}$	29 ± 0.6^{ab}	24 ± 0.6^{bc}	15 ± 0.2^{de}
Zn	$\begin{array}{c} 0.69 \pm \\ 0.27^{b} \end{array}$	$\begin{array}{l} \textbf{0.75} \pm \\ \textbf{0.15}^{ab} \end{array}$	1.4 ± 0.1^{ab}	0.39 ± 0.29^{b}	1.4 ± 0.1^{ab}	$\begin{array}{l} 0.67 \pm \\ 0.07^{ab} \end{array}$	1.4 ± 0.5^{ab}	$\begin{array}{c} \textbf{0.53} \pm \\ \textbf{0.02}^{b} \end{array}$	$\begin{array}{c} 1.7 \pm \\ 0.01^{ab} \end{array}$	3.4 ± 0.1^a
NO ₃ -N	$\begin{array}{c} \textbf{28.7} \pm \\ \textbf{2.9}^{\text{a}} \end{array}$	15.9 ± 0.9^a	0.25 ± 0^{b}	5.8 ± 0.3^{ab}	0.25 ± 0^{b}	1.1 ± 0.1^{ab}	0.25 ± 0^{b}	$0.25 \pm 0.01^{\rm b}$	$0.25 \pm 0.02^{\rm b}$	$0.25 \pm 0.02^{\rm b}$
NH ₄ -N	1.7 ± 0.6^{ef}	$2.9 \pm 0.3^{ m cdef}$	$\textbf{7.4} \pm \textbf{1.2}^{ab}$	$1.4 \pm 0^{\text{def}}$	$13.5\pm1.0^{\text{a}}$	3.9 ± 0.3^{bcde}	4.8 ± 0.5^{bcd}	$1.3\pm0.01^{\rm f}$	5.9 ± 0.3^{bc}	7 ± 0.2^{ab}
C_{WEOC}	288 ± 11^a	237 ± 56^{ab}	188 ± 49^{ab}	170 ± 55^{ab}	164 ± 9^{ab}	272 ± 31^a	$114\pm7^{\rm b}$	218 ± 6^{ab}	141 ± 6^{ab}	147 ± 15^{ab}
Norg	$12.8\ \pm$ 0.9^a	$17.5 \pm \\4.6^{ab}$	$\begin{array}{c} 10.5 \pm \\ 0.7^{ab} \end{array}$	8.8 ± 0.3^{ab}	8.2 ± 0.5^{b}	9.9 ± 0.6^{ab}	9.5 ± 0.3^{ab}	8.9 ± 0.1^{ab}	9.7 ± 0.1^{ab}	9.9 ± 0.2^{ab}
DNA biomass (ng g^{-1})	$883 \pm \\146^{ab}$	575 ± 336 ^{ab}	28 ± 13^{b}	119 ± 38^{b}	1156 ± 30^{ab}	$\begin{array}{c} 802 \pm \\ 106^{ab} \end{array}$	$1102 \pm \\11^{ab}$	883 ± 0^{ab}	1469 ± 1^a	429 ± 1^{ab}
Bacterial richness	821 ± 99 ^{ab}	852 ± 134 ^{ab}	604 ± 67^{ab}	$\begin{array}{l} 459 \pm \\ 366^{\mathrm{b}} \end{array}$	533 ± 72^{b}	779 ± 91^{ab}	618 ± 14^{ab}	724 ± 95^{ab}	$732 \pm \\145^{ab}$	934 ± 81^a
Shannon index - bacteria	5.6 ± 0.1^{ab}	5.5 ± 0.2^{abc}	$\begin{array}{l} 5.2 \pm \\ 0.1^{abcd} \end{array}$	3.5 ± 0.9^{d}	5.1 ± 0.8^{bcd}	5.7 ± 0.1^{ab}	$5.2\pm0.2^{ m abcd}$	4.9 ± 0.2^{cd}	5.6 ± 0.3 ^{abc}	5.7 ± 0.2^a
Fungal richness	51 ± 10^{ab}	37 ± 4^{ab}	23 ± 15^{ab}	22 ± 9^{ab}	14 ± 10^{b}	56 ± 1^a	41 ± 41^{ab}	15 ± 6^{ab}	27 ± 3^{ab}	53 ± 23^{ab}
Shannon index -	$3.3\pm0.3^{\text{a}}$	1.9 ± 0.3^{a}	$2.0\pm1.3^{\text{a}}$	1.7 ± 0.8^a	1.9 ± 0.8^{a}	$3.3\pm0.1^{\text{a}}$	2.8 ± 1.0^{a}	$1.8\pm0.3^{\text{a}}$	2.7 ± 0.1^a	$3.3\pm0.3^{\text{a}}$
fungi										

bacterial/archaeal community structure driven by *stockpile layer* (Stress = 0.11, PERMANOVA $R^2 = 0.85$, p < 0.001) (Fig. S1-A), with a weaker but significant effect of *core* ($R^2 = 0.13$, p < 0.001). When analyzing all three soil categories together (*Start soil, Plant-affected soil*, and *Control soil*; Stress = 0.18), distinct clustering patterns emerged, with *Start soils* clustering below the -0.5 value on the NMDS2 axis (Fig. S1-B). Both *stockpile layer* and *category* significantly impacted the bacterial/archaeal community composition, with R^2 values of 0.55 and 0.11, respectively (Fig. S1-B). In contrast, NMDS plots for the fungal community had high stress values (> 0.25), with lower R^2 (p < 0.001) values than bacteria/archaea for soil layer depth (Fig. S1-C and D) and very little effect of the soil category (Fig. S1-D).

Eighteen bacterial and archaeal phyla were the most prevalent (relative abundance >1 %) in the stockpile layers, out of 54 identified phyla. Nine exceeded 5 % relative abundance, including *Actinobacteriota*, *Proteobacteria*, *Acidobacteriota*, *Fimicutes*, *Chloroflexi*, *Myxococcota*, *Halobacterota*, *Euryachaeota*, and *Armatimonadota*. Fourteen phyla showed significant variation across the stockpile layers, with *Acidobacteriota*, *Actinobacteriota*, and *Chloroflexi* more abundant in top layers (1–5 m) (Fig. S2-A). In contrast, *Armatimonadota*, *Firmicutes*, *Halobacterota*, and *Spriochaetota* were present in increased proportions in the following L3_(5-7m) layer. Two archaeal phyla, *Crenarchaeota* and *Euryarchaeota*, had the highest relative abundance in the deepest stockpile layer L10_(25-28m), while the lowest abundance was observed in L8 (15-18m). For L4_(6-10 m), *Bacteroidota*, *Euryarchaeota*, *Halobacterota*, *MBNT15*, and *Spirochaetota* had the lowest abundance, while *Proteobacteria* showed a significant dominance and *Verrucomicrobiota* had the

highest relative abundance compared to other layers. We identified 25 distinct phyla, mostly found in L8_(15-18m) (eight phyla), L2_(2-5m) and L10_(25-28m) (four phyla each; Fig. S2-A). *Myxococcota* stood out as the only phylum with a relative abundance >1 %, showing significant variation, and being uniquely distinct, as it appeared only in L5_(8-12m).

At order level, 46 taxa were identified with relative abundance >1 %, 34 of which were significantly different across the stockpile layers (Fig. S2-B). The most noticeable changes were observed for Vicinamibacterales and the 11-24 order within Acidobacteriota; Rhizobiales and Methylococcales within Proteobacteria; Streptosporangiales, Micromonosporales, and Microtrichales within Actinobacteriota; and Bacillales and Hydrogenispora within Firmicutes. Among these, the highest proportions of Methylococcales were found in $L4_{(6-10m)}$ and $L8_{(15-18m)}$, while Hydrogenispora were most prevalent in L3_(5-7m) and L5_(8-12m). Bacillales proportions increased with depth, whereas Streptosporangiales, 11-24, and Rhizobiales generally decreased. However, at a depth of 15-18 m (L8), Rhizobiales had the highest relative abundance among all soil layers. In total, 128 distinct orders were identified, with only eight having a relative abundance >1 % in at least one soil layer. Among these, Micrococcales, Mycoplasmatales, and Methanocellales stood out as both distinct and significantly different, being also most abundant in $L2_{(2-5m)}$, $L4_{(6-10m)}$, and $L7_{(13-15m)}$, respectively.

Most fungal organisms belonged to *Ascomycota* and *Basidiomycota*, which were the only phyla whose relative abundance differed significantly between the soil layers (Fig. S3-A). At the order level, nine orders with relative abundances >1 % showed significant differences. These included *Sordariales*, *Pleosporales*, *Hypocreales*, *Pezizales*, *Capnodiales*,

and *Helotiales* within the phylum *Ascomycota*, as well as *Russulales*, *Polyporales*, and *Trichosporonales* within the phylum *Basidiomycota* (Fig. S3-B). Overall, the relative abundance of orders varied across layers without a clear pattern, however, higher proportion of *Polyporales* was found in $L1_{(1-4m)}$ and $L8_{(15-18m)}$, of *Pleosporales* in $L3_{(5-7m)}$, and of *Russulales* in $L3_{(5-7m)}$, $L9_{(20-25m)}$, and $L10_{(25-28m)}$.

FAPROTAX identified bacterial/archaeal functions significantly differing across the stockpile soil layers (Fig. 2). Nitrogen cycle-related functions dominated the top L1_(1.4m) and L6_(12·13m) layers, while C cycling was more prominent in L7_(13·15m) and L10_(25·28m). Sulfur respiration, as well as Mn and Fe metabolisms were prevalent in deeper layers (L8, L9, and L10; 15-28 m), with occasional S oxidation in the top layer. Notably, L8_(15·18m) exhibited the most pronounced functional activity related to the dark oxidation of thiosulfate, sulfur, sulfide, and other S compounds. L4_(6·10m) layer had the highest abundance of ureolysis and cellulolysis functions. Other functions were scattered across the layers without particularly noticeable trends. No significant functional differences were identified by FUNGuild for fungal organisms across the layers.

3.3. Germination and plant performance

At the species level (including both *A. lentiformis* populations), the highest germination % (62 %) was observed in L7_(13-15m), followed by percentages exceeding 50 % in L2, L3, L4 (2–10 m), and L6_(12-13m). In contrast, the lowest germination (< 20 %) was in the 15 to 25 m layers

(L8 and L9). Seedling survival peaked in L4 $_{(6\text{-}10\text{m})}$, L1 $_{(1\text{-}4\text{m})}$, L3 $_{(5\text{-}7\text{m})}$, L2 $_{(2\text{-}6\text{m})}$, and L8 $_{(15\text{-}18\text{m})}$, ranging from 80 % to 95 % (Fig. 3, Table S1). Notably, no seedlings survived in the L9 $_{(20\text{-}25\text{m})}$ layer, and seedling mortality exceeded 55 % in L6 $_{(12\text{-}13\text{m})}$ and L10 $_{(25\text{-}28\text{m})}$ layers. The highest final number of plants was in the 1 to 10 m (L1, L2, L3, and L4) and 13 to 15 m (L7) layers (Table S1).

Pronounced differences in seed germination, seedling survival, and mortality were observed between the two *A. lentiformis* populations (Table S2). Overall, NM-PHX showed a higher mean germination % than M-IK (48 % vs. 38 %) but also had a higher mean seedling mortality (36 % vs. 30 %). The highest mortality for M-IK seedlings occurred in the $L6_{(12-13m)}$ layer (57 %), while for NM-PHX, it was in $L10_{(25-28m)}$ (86 %). However, both populations had very similar final plant counts, with 61 NM-PHX plants and 57 M-IK plants.

At harvest, significant differences in plant performance were observed across the stockpile's soil layers. At the species level, the largest plants, measured by mean root length, leaf area, height, and fresh biomass, the L1 $_{(1-4m)}$ layer (Fig. 4, Table S3), followed by L2 $_{(2-5m)}$, L4 $_{(6-10m)}$, and L3 $_{(5-7m)}$. Note that no viable plants were obtained from the L9 $_{(20-25m)}$ layer. No significant differences in mean root length were observed between soil layers during the first 14 days after germination (Fig. 4). By day 21, significant differences emerged and persisted until the end of the experiment. The most consistent root growth was found in the layers from 1 to 7 m, while minimal root growth occurred in L5, L6, L7, L8 (8–18 m), and L10 $_{(25-28m)}$ layers (Tables S3, S4). Despite no significant differences in root length between populations at harvest, a

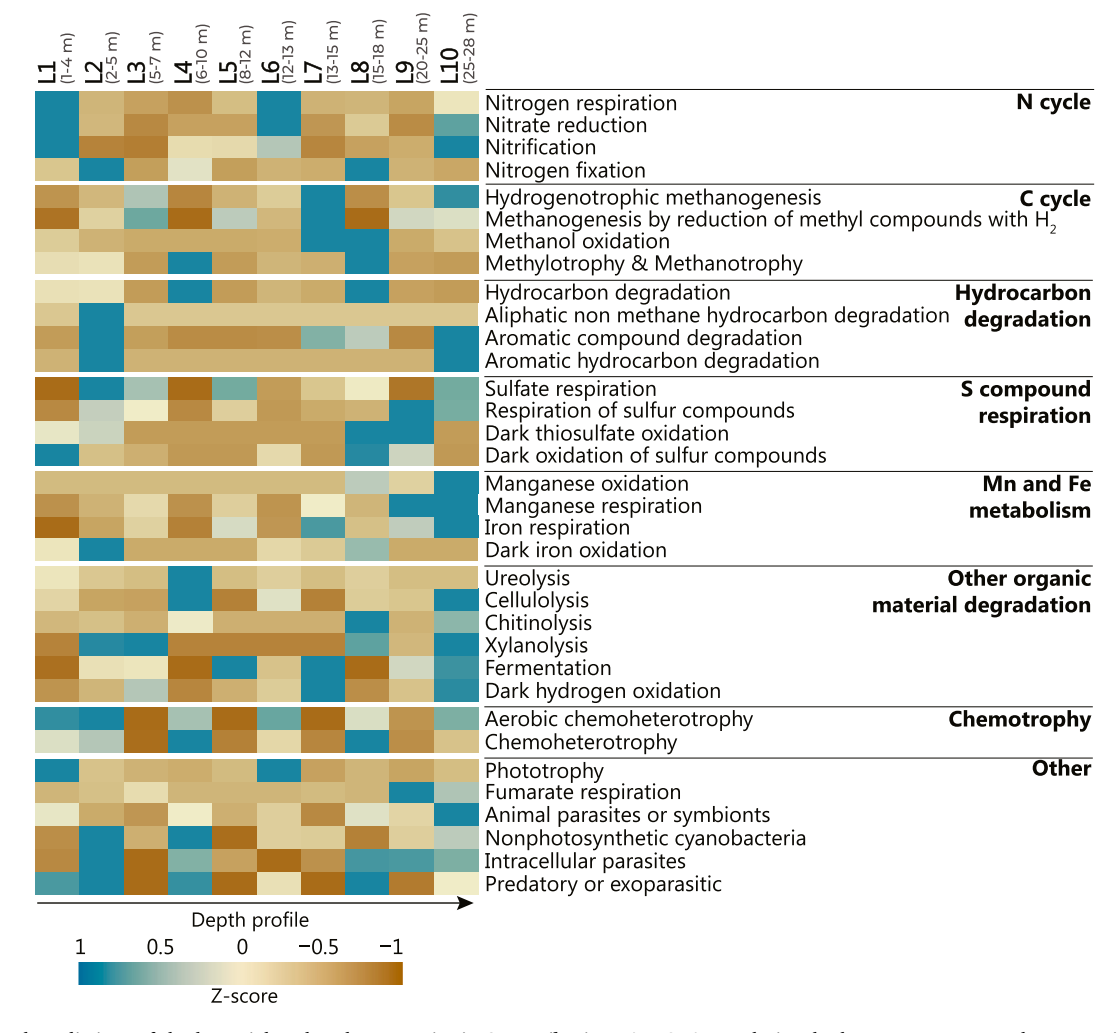


Fig. 2. Functional predictions of the bacterial/archaeal community in *Start soil* using FAPROTAX analysis. The heatmap represents the proportion of significant functional groups across stockpile depth layers. The data was normalized using z-score scaling.

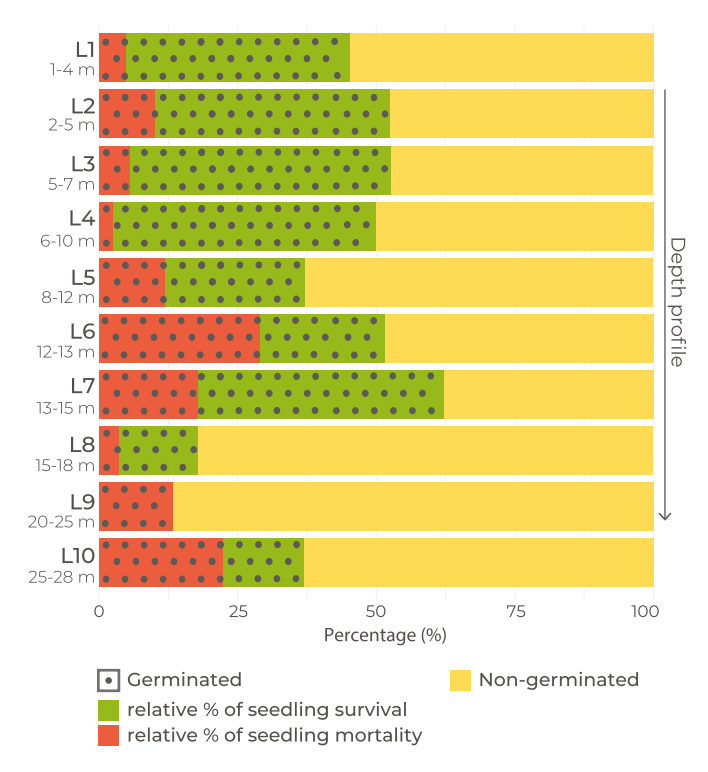


Fig. 3. Germination, seedling survival, and seedling mortality patterns of *A. lentiformis* across stockpile layers (*Start soil*). The bars show the percentages of germinated (dotted area) vs. non-germinated (yellow) seeds, along with the relative percentages of seedling survival (green) and mortality (red). The layers are presented in descending order from top (L1) to bottom (L10) of the stockpile.

nested ANOVA revealed variations in root growth rate between populations across L2_(2-5m), L3_(5-7m), L5_(8-12m), L7_(13-15m), and L10_(25-28m) layers (Table S5). The M-IK population excelled in L2_(2-5m), L3_(5-7m), and L10_(25-28m), while the NM-PHX performed better in L5_(8-12m) and L7_(13-15m).

Concentrations of P, K, S, Ca, and Mg in shoot samples were mostly within normal ranges, though variations occurred by soil layer and plant population (Table S6). Sulfur was relatively high in both populations in L8_(15-18m), and in M-IK population in L7_(13-15m), L3_(5-7m), and L10_(25-28m). Iron concentrations increased 10–100-fold in plants grown in layers below 8 m, exceeding 8000 mg kg⁻¹ in M-IK population in L7_(13-15m) and L5_(8-12m). Copper exceeded 50 mg kg⁻¹ in L5_(8-12m) and L6_(12-13m) layers for both populations and in L3_(5-7m) and L7_(13-15m) layers for M-IK plants, while Zn surpassed 200 mg kg⁻¹ in M-IK plants in L3_(5-7m), L5_(8-12m), L6_(12-13m), L7_(13-15m), and L10_(25-28m). Manganese concentration of 500 mg kg⁻¹ or higher was found in both populations in L5_(8-12m), and in M-IK plants from L3_(5-7m) and L10_(25-28m).

3.4. Associations between soil properties and germination, plant establishment, and performance metrics

PLS models assessing link between soil abiotic and biotic variables with germination and plant establishment (number of plants that survived through the entire experiment) explained 83 % of the variation in Germination %, and 82 % of the variation in final plant count, i.e., successful plant establishment. In each model, 14 and 12 explanatory variables were identified as significantly important (VIP > 1), respectively (Fig. 5). Regarding plant performance, the models explained 59 % of the variation in leaf area, and 65 % in total root length, with 21 and 23 explanatory variables significantly contributing to the variance in these traits, respectively (Fig. 6, Table S7).

Among abiotic factors, Mn, Mg and Zn concentration had the

strongest negative influence on germination and plant establishment (Fig. 5). Regarding biotic factors, significant microorganisms identified at various taxonomic levels were limited to four bacterial phyla (Actinobacteriota, Chloroflexi, Firmicutes, and MBNT15) and two fungal phyla (Ascomycota and Basidiomycota). Positive associations were observed only within the Ascomycota phylum for number of successfully established plants, and Cladosporiaceae family within the same phylum for Germination %. The *Basidiomycota* phylum and all significant bacterial taxa had negative associations with germination and plant establishment metrics. Bacillaceae and Planococcaceae families from the Firmicutes phylum as well as Anaerolineales (o) and Anaerolineaceae (f) within Chloroflexi were identified in both PLS models. Additionally, Micromonosporales (o) and Micromonosporaceae (f) within Actinobacteriota, and the candidate phylum MBNT15 were linked only with germinations. Notably, bacterial richness was negatively associated with the number of successfully established plants.

Plant performance was strongly associated with soil abiotic parameters and bacterial/archaeal organisms, while no fungal taxa were identified as explanatory variables in PLS models for leaf area and root length (Fig. 6). The majority of identified variables overlapped in both models (20 out of 24 variables) and were positively associated with the examined parameters (except for Actinobacteriota phylum negatively associated with root length). Among the abiotic parameters, Ca:Mg ratio and the top layer of the stockpile (L1_(1-4 m)) were the most strongly associated with improved plant performance. The majority of identified microbial organisms belonged to Planctomycetota, Acidobacteriota, Proteobacteria, Verrucomicrobiota, and Firmicutes. Within these phyla, the Vicinamibacterales and 11-24 orders from Acidobacteriota, the Thermoactinomycetales order from Firmicutes, the Steroidobacterales order from Proteobacteria, and the Gemmatales order from Planctomycetota were all positively associated with both plant traits. Interestingly, plant metrics were also strongly associated with archaea, particularly organisms within the Crenarchaeota phylum, specifically from the Nitrososphaerales order.

3.5. Effect of plants and water on soil properties at harvest

The impact of watering and the presence of plants on the biochemical properties of stockpile soil layers after a 9-week experiment in rhizoboxes was assessed by comparing 22 parameters of the Control and Plantaffected soils with the characteristics of the Start soil (Table S8). While only 5 to 8 parameters changed in the upper soil layers (up to 10 m), more significant changes were observed in the deeper layers, where 8 to 15 parameters differed from the Start soil, with the most notable alterations occurring in L8 and L9 (15 to 25 m). The concentration of NO₃-N was the most significantly affected parameter, decreasing across all layers after both watering and plant growth (except for L5(8-12m) in the presence of plants). Other frequently affected parameters, such as Mn, NH₄-N, and bacterial Shannon index, also decreased across six soil layers following both watering and plant growth. Additionally, bacterial and archaeal richness declined relative to the Start soil in deeper layers. Conversely, levels of S, Ca, Ca:Mg, Na, CWEOC, Norg, DNA biomass, and fungal richness generally increased. Notably, OM% and fungal Shannon index were unaffected by both watering and plant growth.

Regarding microbial communities, differences in the relative abundance proportions of various phyla and orders between soil layers diminished after 9 weeks of the experiment, as observed for both bacterial/archaeal and fungal phyla (Figs. S4 and S5). For bacterial/archaeal phyla, there was a notable increase in the proportion of organisms from *Actinobacteriota* and *Proteobacteriota*, along with a decrease in *Firmicutes*. For fungal phyla, the proportion of *Basidiomycota* organisms decreased after the experiment.

The proportions of key microbial taxa that explained variation in germination and plant performance metrics (identified in the PLS analysis), also changed significantly after watering and plant growth (Table S9). Several taxa with a negative impact on germination, such as

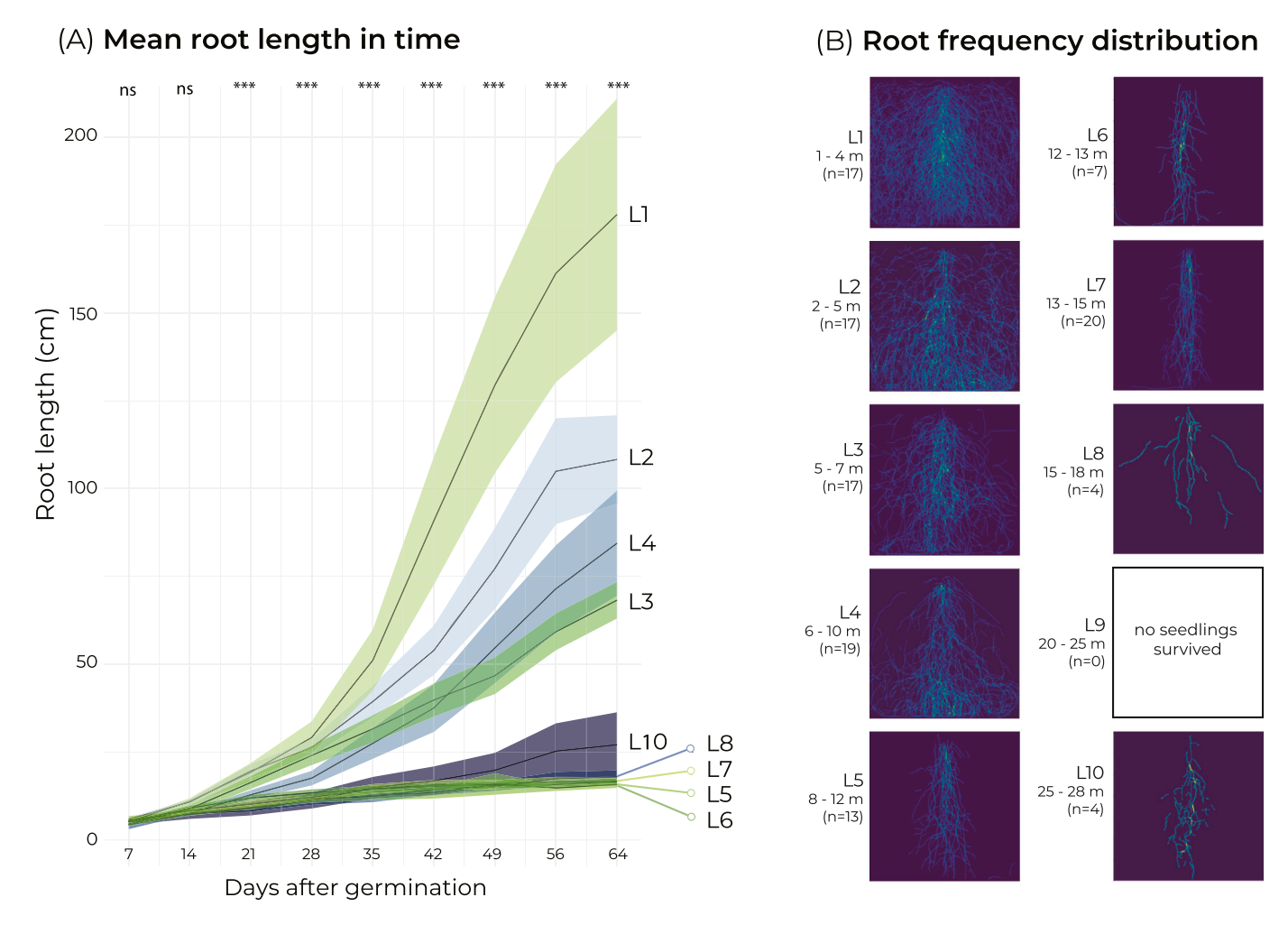


Fig. 4. Root system development of *Atriplex lentiformis* in rhizoboxes filled with stockpile soil layers. (A) Temporal changes in mean total root length (cm) observed over 64 days (9-weeks) from germination. Lines represent the mean values \pm SE (shaded areas). For each of the 9 measurement points, differences in mean root length across soil layers were tested using the Kruskal-Wallis test with Bonferroni correction (***, p-value \leq 0.001; ns, not significant). (B) Root frequency distribution visible on the inner sides of the rhizoboxes at harvest.

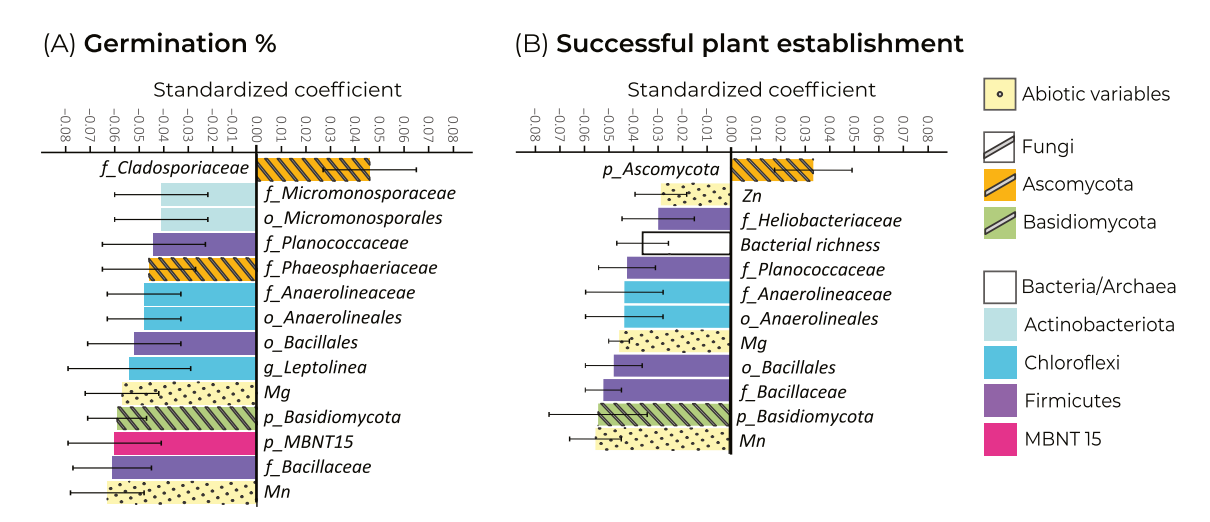


Fig. 5. PLS regression of soil factors influencing germination and plant survival. Partial Least Squares (PLS) regression analysis of abiotic and biotic factors of stockpile soil layers, influencing (A) Germination % and (B) successful early plant establishment (represented by the number of plants that survived through the entire experiment). Key explanatory variables, identified by a Variable Importance in Projection (VIP) score greater than 1.0, are organized in descending order based on their standardized regression coefficients (\pm SD). Taxonomic hierarchy levels preceding the names of microbial taxa are denoted as: p for phylum, o for order, f for family, and g for genus.

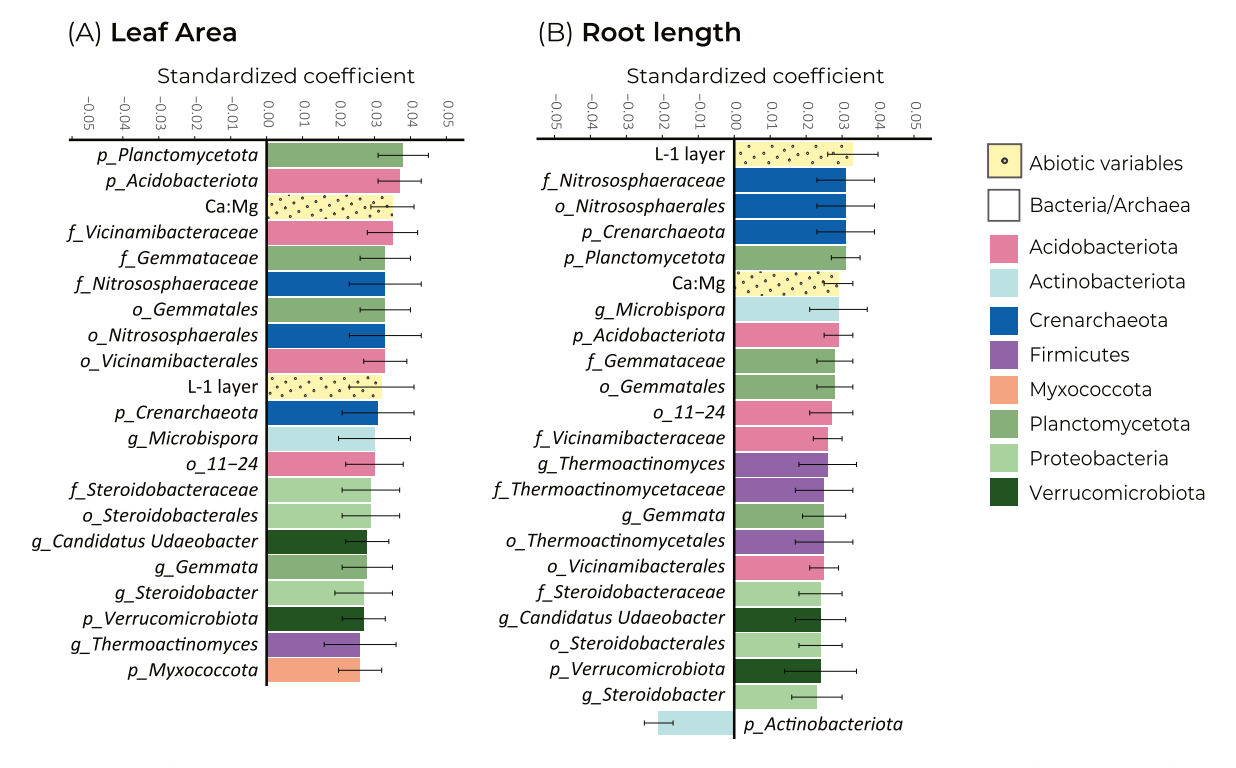


Fig. 6. PLS regression of soil factors influencing plant performance. Partial Least Squares (PLS) regression analysis of abiotic and biotic factors influencing (A) leaf area and (B) root length in plants growing in stockpile soil layers. Key explanatory variables, identified by a Variable Importance in Projection (VIP) score greater than 1.0, are organized in descending order based on their standardized regression coefficients (\pm SD). Taxonomic hierarchy levels preceding the names of microbial taxa are denoted as: p for phylum, o for order, f for family, and g for genus.

Anaerolineaceae (f), Anaerolineales (o), MBNT15 (p), Leptolinea (g), Heliobacteriaceae (f), Bacillales (o), and Basidiomycota (p), showed a decline in their relative abundance, especially in the deeper layers of the stockpile. In contrast, the proportion of organisms within the Ascomycota phylum, positively associated with germination, significantly increased. However, the abundance of some negatively associated taxa, such as Micromonosporaceae (f), Micromonosporales (o), Phaeosphaeriaceae (f), and Basidiomycota (p) also increased. For microorganisms positively associated with plant establishment and with leaf area and root length, such as Gemmata (g), Gemmataceae (f), Steroidobacter (g), Vicinamibacteraceae (f), and Vicinamibacterales (o), showed increased abundance. Interestingly, Crenarchaeota organisms, along with the Nitrososphaeraceae (f) and Nitrososphaerales (o), declined in abundance. A decrease was also noted in Thermoactinomycetaceae (f) and Thermoactinomycetales (o).

The changes in relative abundance were also reflected in shifts in the functional predictions of microbial communities in both *Control* and *Plant-affected* soils (Fig. S6). Nitrification decreased after watering and plant growth, particularly in L6_(12-13m), L9_(20-25m), and L10_(25-28m). Conversely, denitrification, aerobic chemoheterotrophy, and phototrophy activities increased in most soils compared to *Start* soil. Iron and Mn respiration generally declined across all soil layers. Additionally, the mean amplicon sequence variant (ASV) counts generally increased after the experiment (Table S10). While the increase in bacterial/archaeal organisms was similar for both *Plant-affected* and *Control* soils, the increase in fungal organisms was more pronounced in the presence of plants. Overall, the growth of *A. lentiformis* influenced soil properties and microbial community structures, although differences between the two populations were marginal.

4. Discussion

4.1. Impact of long-term stockpiling on biochemical characteristics of topsoil across depth layers

Our findings demonstrate that long-term soil stockpiling leads to substantial vertical heterogeneity in biochemical properties and microbial community structure. This spatial complexity likely reflects the formation of aerobic, transition, and anoxic zones – a pattern consistent with prior stockpile studies (Abdul-Kareem and McRea, 1984; Hernandez et al., 2024). However, the irregular microbial distribution and biochemical similarities between non-adjacent layers highlight how stockpile heterogeneity - possibly due to uneven compaction and material sorting – disrupts any predictable stratification. While the upper 5 m showed signatures of aerobic conditions, including elevated NO₃-N and CWEOC concentrations, and greater presence of aerobic chemoheterotrophs, phototrophs, and aerobic nitrogen-cycling taxa (e.g., Rhizobiales), similar biochemical and microbial traits reappeared unexpectedly at deeper levels (e.g., $L6_{(12-13m)}$). The presence of taxa such as Acidobacteriota group 11-24, Streptomycetales, and Streptosporangiales within those zones further reflects adaptation to nutrient-poor, semiarid conditions - characteristics likely exacerbated by prolonged soil storage.

Signs of anaerobic conditions emerged already within the 1–5~m range, with increased abundance of anaerobic and extremophilic taxa (e.g., S085~[Chloroflexi], Thermomicrobiales), typically associated with oligotrophic and arid environments, and with soil organic carbon fractions (Petriglieri et al., 2018). Peaks in C_{WEOC} levels and abundance of Microtrichales (Actinobacteriota phylum) in aerobic zones also point to active carbon mineralization (Sarula et al., 2023), further indicating that oxygen limitation can develop relatively close to the surface.

Below 5 m, distinct anoxic pockets (e.g., $L3_{(5-7m)}$, $L5_{(8-12m)}$, $L7_{(13-15m)}$, $L9_{(20-25m)}$, $L10_{(25-28m)}$) were characterized with active hydrogenotrophic methanogenesis (high abundance of *Methanobacteriales*,

Methanocellales, and Methanosarciniales), sulfate reduction and respiration (Desulfitobacteriales and Desulfotomaculales orders) (Choi et al., 2022; Karnachuk et al., 2023), along with decomposers like Bacteroidales, Clostridiales, and Veillonellales-Selenomonadales (Palmer et al., 2019). This community composition reflects active anaerobic organic matter decomposition and reduced nitrogen turnover, as indicated by NH₄-N accumulation and reduced NO₃-N availability.

Interestingly, layers L4_(6-10m) and L8_(15-18m), displayed distinct microbial signature, marked by increased methylotrophic, reduced hydrogenotrophic methanogenesis, and elevated abundance of methane-oxidizing *Proteobacteria*, suggesting the presence of micro-oxic conditions with methane enrichment. These transitional zones could facilitate methane oxidation above anoxic zones where methane diffuses upward. Indeed, methylotrophs such as *Methylococcales*, metabolize single-carbon compounds, like methane, and thrive in ecosystems with methane influx, using it as their sole energy source (Chistoserdova and Kalyuzhnaya, 2018).

Two factors likely contribute to the formation of these distinct biochemical zones below 5 m. First, variable oxygen diffusion - potentially due to uneven rock distribution and reduced soil compaction – creates localized micro-oxic environments that alter gas exchange. Second, contrasting OM% influences microbial metabolism, with lower OM% (<0.6 %) in micro-oxic layers indicating enhanced OM degradation, while higher OM% in anoxic pockets (1.2 % to 1.8 %) reflect slower decomposition. Variations in Fe content further differentiate these zones. Elevated Fe levels in anoxic layers may reflect both microbial production of ferredoxin, an iron-sulfur protein essential for hydrogenotrophic methanogenesis, and Fe reduction process, indirectly favoring hydrogenotrophy, as Fe can serve as an alternative electron acceptor for aerobic methanotrophs under low-oxygen conditions (Zheng et al., 2020). Conversely, limited Fe availability in micro-oxic conditions may reduce ferredoxin synthesis, hindering electron transfer processes critical for hydrogenotrophic methanogenesis. As a result, microbes in these layers might adjust their metabolic pathways, relying less on Fe-dependent processes and favoring methylotrophy instead (Ebrahimian et al., 2023).

4.2. Germination and early plant establishment are driven by different biophysical characteristics of stockpile soil layers

The findings reveal a notable decoupling between germination patterns and subsequent plant performance across stockpile soil layers. This divergence suggests that germination and early plant development are governed by different biophysical and microbial drivers, underscoring the importance of evaluating multiple plant response stages when assessing stockpile viability for reclamation. Germination success was primarily linked to biotic factors, especially fungal communities. Positive associations with Ascomycota and Cladosporiaceae suggest these taxa may facilitate germination through phytohormone-mediating signaling. Ascomycota, for instance are known to produce gibberellins (GAs) that aid in breaking seed dormancy (Ogawa et al., 2003), while Cladosporiaceae members, often identified as plant endophytes or saprobic fungi, may enhance germination through secondary metabolites like indole-3acetic acid (IAA), promoting plant growth and suppressing pathogens (Pan et al., 2023). These findings point to a supportive microbial niche in specific layers that favor seed activation.

In contrast, several microbial taxa abundant in anoxic zones and micro-oxic pockets showed negative associations with germination. For instance, the *Anaerolineales* family (*Chloroflexi*), known as strict anaerobes involved in fermentation processes, may produce allelopathic metabolites, such as acetate, ethanol, and lactate that inhibit germination and seedling development (Chen et al., 2023; Freches and Fradinho, 2024). The *Leptolinea* genus within this group, produces terpenoids, that can either promote growth via plant hormones or inhibit germination through allelopathy (Zhao et al., 2009). Their syntrophic relationship with hydrogenotrophic methanogens likely supports its abundance in

anoxic layers (Yamada et al., 2006).

Germination suppression was also linked to microbial assemblages characteristic of deeper, strongly anoxic layers of the stockpile. These communities included facultative and obligate anaerobic bacteria, phototrophs, and spore-forming taxa (e.g., *Planococcaceae*, *Heliobacteriacea*, *Micromnosporales*) adapted to low-oxygen, compacted conditions (Madigan et al., 2017). Although some of these taxa participate in S cycling, their distribution was linked more strongly with soil redox status than with S availability, indicating redox potential as the dominant control (Spring and Rosenzweig, 2006). Moreover, negative associations with *Basidiomycota*, a diverse fungal phylum encompassing endophytic, allelopathic and saprotrophic lineages, raise the possibility of fungal secondary metabolites inhibiting early seedling development in these zones (Rungjindamai and Jones, 2024).

Among abiotic factors, Mn and Mg concentrations emerged as critical inhibitors of germination. Both elements can disrupt phytohormone signaling and hinder germination. Manganese, especially at levels exceeding 400 mg ${\rm kg}^{-1}$, may interfere with IAA biosynthesis, and its reduction to bioavailable Mn (II) in anoxic zones could induce oxidative stress and nutrient uptake disruptions in seedlings (Takagi et al., 2021). Similarly, Mg, that in our study tended to accumulate in deeper layers, was also linked to germination inhibition, consistent with its known toxicity at high concentrations, particularly in salt form.

Plant growth data suggest that only the upper 10 m of the stockpile provided favorable conditions to plant establishment. Below this depth, growth was markedly reduced and root elongation severely inhibited. These patterns likely reflect shifting biophysical constraints, including altered redox status, compaction, and elemental availability. Notably, elevated Fe accumulation in plants from mid-depth layers may signal increased Fe availability under anoxic conditions. While essential, excessive Fe uptake may cross toxicity thresholds, disrupting physiological processes. Indeed, the accumulation of high Fe levels in anoxic layers was previously reported as a key factor hindering the potential of stockpile soils to support plant growth (Abdul-Kareem and McRea, 1984; Ledesma et al., 2025). Similarly, the peak in plant S content corresponded with elevated soil S in specific layers, suggesting microbial mediation of Fe and S availability across various stockpile depths.

Notably, bacterial and archaeal taxa were the most consistent positive predictors of plant leaf and root length growth. These microbial groups likely contribute to stress tolerance during early growth stages. Archaea may play vital roles through auxin biosynthesis (e.g., IAA) and improved nutrient supply, particularly via ammonia oxidation and phosphorus solubilization (Taffner et al., 2018). Emerging evidence also implicates *Planctomycetota* as pioneer root-surface colonizers that participate in carbon turnover, potentially aiding in plant establishment in disturbed or nutrient-poor soils (Godinho et al., 2024). Among abiotic soil parameters, the Ca:Mg ratio was the only driver positively influencing plant growth. A balanced Ca:Mg ratio is known to promote plant biomass productivity, and may boost phytoremediation efficiency in metal-accumulating plants, underscoring its importance for post-mining site remediation projects (Mleczek et al., 2012).

4.3. Optimizing stockpile recovery: plant-soil feedback and strategies to overcome soil heterogeneity

Assessing recovery dynamics through plant-soil feedback (PSF) revealed that both abiotic and microbial properties shifted in response to plant presence in the soil. However, underlying depth-dependent heterogeneity within the stockpile persisted. Over the 9-week period, microbial abundance patterns began to converge across depth layers, with functional signatures typical of deeper layers – such as Fe and Mn respiration and S metabolism – declining after the experiment. This flattening of microbial functional differentiation, along with an increase in mean ASV counts, likely reflects improved aeration and moisture availability due to watering and root-mediated effects, potentially enhancing soil functionality. While these shifts signal early signs of

recovery, the pace and extent of improvement are likely constrained by the initial substrate quality and stockpile layer, both of which can shape revegetation outcomes. This suggests that short-term interventions may be insufficient to overcome the legacy effects of stockpile-induced stratification

Bacterial/archaeal and fungal communities responded differently to PSF, highlighting their differing ecological roles during early restoration and complex temporal dynamics of PSF (Thakur et al., 2021). While bacterial/archaeal richness and diversity tended to decline, fungal communities displayed a notable recovery, reaffirming their importance in early stages of soil restoration. The selective advantage for fungi may stem from their ability to persist and interact with plants under resourcelimited conditions. Mycorrhizal associations, in particular, are wellknown to enhance plant resilience and nutrient acquisition under stress through positive feedback loops (Zhu et al., 2021). The observed fungal expansion may also stem from their low host specificity and ability to rapidly adapt to changing root exudate profiles, aiding plant survival in challenging environments (van der Heyde et al., 2020). These microbial responses could reflect either the initial stages of soil conditioning or a 'lag effect' in PSF dynamics, a phenomenon frequently reported in degraded ecosystems (Gundale and Kardol, 2021). Although it remains uncertain whether early plant-driven soil conditioning in degraded stockpile soils will lead to positive or negative feedback loops, the trajectory of these interactions will be critical for the long-term success of plant community establishment in reclamation projects.

Although, selecting metal-tolerant plant ecotypes is often recommended for revegetation - particularly when shallow capping layers allow root penetration into underlying contaminated substrates (Dietrich et al., 2021) - our results suggest that metal tolerance alone may not ensure successful establishment in stockpile soils. The minimal performance differences between A. lentiformis accessions from contrasting metalliferous and non-metalliferous habitats likely reflect the relatively low metal concentrations in this particular stockpile. However, the metallicolous population (M-IK) showed a tendency toward increased Zn accumulation, suggesting either a greater internal Zn demand or a distinct ionomic strategy - potentially adaptive traits shaped by its native environment. This aligns with recent findings showing Zn hotspots in M-IK A. lentiformis seeds, supporting population-level variability in metal tolerance and accumulation relevant to early seedling establishment in this species (Murawska-Wlodarczyk et al., 2024). Similar patterns have been observed in the metal-tolerant model species Arabidopsis halleri, where enhanced Zn accumulation in vegetative tissues of certain populations was linked to increased Zn provisioning to seeds, potentially benefiting seedlings development (Babst-Kostecka et al., 2020). Despite its known stress tolerance, robust root system and strong performance in metal-contaminated environments, A. lentiformis struggled to establish well in the stockpile soils, suggesting it may not be suitable as first-introduced species on poor quality stockpile soils (Mendez et al., 2007). This reduced performance likely reflects the severely degraded stockpile conditions and disturbed microbial networks, underscoring that successful establishment requires restoration strategies finely tuned to local site constraints. In contrast, the use of fast pioneer grasses or ruderal species, may be more effective in initiating recovery and conditioning soil for later successional species (Randelovic et al., 2024).

The persistent biogeochemical heterogeneity observed across depth layers emphasizes the critical role of stockpile construction process in shaping long-term soil functionality and capacity to support plant establishment. Although X-ray mineral analysis point to a common parent material across all layers (Ledesma et al., 2025), stark differences in nutrient levels and microbial profiles suggest that heterogeneity arises primarily from how the material was handled during stockpiling. Overcoming this legacy requires targeted strategies beyond passive revegetation. One potential approach is the intentional mixing of contrasting layers to improve homogeneity and functional balance. For instance, combining N-rich with C-rich layers may stimulate beneficial

microbial dynamics and enhance nutrient cycling. Previous work demonstrated improved plant performance after mixing of layers (Mushia et al., 2016), although these trials were limited to shallow layers (< 3 m), leaving the potential deeper interventions unexplored. Alternatively, soil amendments tailored to site-specific constraints could accelerate soil recovery and boost plant resilience, though their selection must align with the chemical and biological profile of each stockpile (Mushia et al., 2016; Soria et al., 2024). Importantly, any amendment strategy could be paired with long-term monitoring to evaluate stability and ecosystem progression.

5. Conclusions

This study evaluated the potential of a 28 m-deep topsoil stockpile for site reclamation by examining A. lentiformis germination and early establishment across its depth profile in a semi-arid environment. It represents one of the few studies to comprehensively link biogeochemical properties of individual layers with early plant and microbial responses across such an extensive stockpile profile. The results highlight that strong vertical heterogeneity in soil chemistry and microbial community structure profoundly influences early plant establishment. Seed germination and plant performance were influenced by distinct sets of variables, reflecting the complex interplay of factors involved in successful revegetation and reclamation efforts. Surface and upper subsurface layers (up to 10 m) demonstrated greater potential to support vegetation, associated with more favorable soil conditions and microbial communities. In contrast, deeper layers were characterized by anaerobic conditions, microbial shifts toward methanogenesis, Fe/Mn cycling, and a higher prevalence of potential plant pathogens - factors that likely contribute to hindered plant establishment in soils from there layers. Notably, plant presence and sustained irrigation induced measurable changes in soil conditions, suggesting that even heavily degraded deep layers may undergo functional recovery. However, the direction and long-term sustainability of these shifts remain uncertain and require continued monitoring.

Given the pronounced heterogeneity and varying degrees of anoxic conditions across the stockpile depth profile, careful attention should be given to topsoil stockpile design, material handling during formation, and strategies for material reuse. A better understanding of the processes driving soil degradation in stockpiles – alongside mitigation strategies such as incorporating coarse materials to improve aeration or monitoring Fe/Mn dynamics – could help preserve topsoil health features and reduce long-term quality loss. Further research should focus on tracking the pace and extent of recovery in stockpiled soils under field condition and across longer timescales to inform scalable and effective restoration approaches. Ultimately, optimizing revegetation in stockpiled soils will require integrated strategies that address both biological and physicochemical constraints. By leveraging insights from plant-soil feedback, microbial dynamics, and vertical soil heterogeneity, more adaptive and ecologically grounded reclamation strategies can be developed.

Supplementary data to this article can be found online at https://doi.org/10.1016/j.scitotenv.2025.180673.

CRediT authorship contribution statement

Kamila Murawska-Wlodarczyk: Writing – original draft, Visualization, Methodology, Investigation, Formal analysis, Data curation, Conceptualization. Priyanka Kushwaha: Writing – review & editing, Investigation, Data curation. Owyn Stokes: Investigation. Craig Rasmussen: Writing – review & editing, Conceptualization. Julia W. Neilson: Writing – review & editing, Supervision, Project administration, Funding acquisition, Conceptualization. Raina M. Maier: Writing – review & editing, Supervision, Project administration, Funding acquisition, Conceptualization. Alicja Babst-Kostecka: Writing – review & editing, Supervision, Project administration, Methodology, Investigation, Funding acquisition, Conceptualization.

Declaration of Generative AI and AI-assisted technologies in the writing process

During the preparation of this work the authors used ChatGPT 40 in order to proofread grammatical structures and punctuation. After using this tool, the authors reviewed and edited the content as needed and take full responsibility for the content of the publication.

Declaration of competing interest

The authors declare that they have no known competing financial interests or personal relationships that could have appeared to influence the work reported in this paper.

Data availability

The raw sequencing data for bacteria/archaea and fungi can be accessed in NCBI's Sequence Read Archive under BioProject PRJNA1180669. Raw soil and plant datasets are available upon request.

Acknowledgements

This work was supported by the National Institute of Environmental Health Sciences Superfund Research Program (Grant number P42ES004940) at the University of Arizona, the University of Arizona; Center for Environmentally Sustainable Mining Industry-Academic Revegetation Research Cooperative; The University of Arizona School of Mining and Mineral Resources, LabEx DRIIHM, French programme 'Investissements d'Avenir' (ANR-11-LABX-0010), managed by the ANR and within the framework of the OHMi Pima County (2022-2023/4). We thank Tomasz Włodarczyk for technical expertise in designing the custom rhizobox system.

References

- Abdul-Kareem, A.W., McRea, S.G., 1984. The effects on topsoil of long-term storage in stockpiles. Plant Soil 76, 357–363.
- Aleksandrova, A.Y., Timofeeva, S.S., 2021. Impact of mining of common minerals on the environment and public health. IOP Conf. Ser. Earth Environ. Sci. 848.
- Amir, H., Bordez, L., Cavaloc, Y., Jourand, P., Ducousso, M., Juillot, F., 2022. Effects of ultramafic topsoil stockpiling during mine activities on its microbial diversity and other microbiological and physicochemical characteristics. Ecol. Eng. 177.
- Babst-Kostecka, A., Przybyłowicz, W.J., Seget, B., Mesjasz-Przybyłowicz, J., 2020. Zinc allocation to and within Arabidopsis halleri seeds: different strategies of metal homeostasis in accessions under divergent selection pressure. Plant Environ. Interact. 1–14.
- Callahan, B.J., McMurdie, P.J., Rosen, M.J., Han, A.W., Johnson, A.J.A., Holmes, S.P., 2016. DADA2: high-resolution sample inference from Illumina amplicon data. Nat. Methods 13, 581.
- Chen, J., Jin, Z., Xiang, L., Chen, Y., Zhang, J., Zhao, J., et al., 2023. Ethanol suppresses rice seed germination through inhibiting ROS signaling. J. Plant Physiol. 291, 154123.
- Chistoserdova, L., Kalyuzhnaya, M.G., 2018. Current trends in methylotrophy. Trends Microbiol. 26, 703–714.
- Choi, B.Y., Park, J., Ham, B., Kirk, M.F., Kwon, M.J., 2022. Effect of CO(2) on biogeochemical reactions and microbial community composition in bioreactors with deep groundwater and basalt. Sci. Total Environ. 807, 150803.
- Cooke, J.A., Johnson, M.S., 2002. Ecological restoration of land with particular reference to the mining of metals and industrial minerals: a review of theory and practice. Environ. Rev. 10, 41–71.
- D'Agui, H.M., van der Heyde, M.E., Nevill, P.G., Mousavi-Derazmahalleh, M., Dixon, K. W., Moreira-Grez, B., et al., 2022. Evaluating biological properties of topsoil for postmining ecological restoration: different assessment methods give different results. Restor. Ecol. 30.
- Dietrich, C.C., Tandy, S., Murawska-Wlodarczyk, K., Banas, A., Korzeniak, U., Seget, B., et al., 2021. Phytoextraction efficiency of *Arabidopsis halleri* is driven by the plant and not by soil metal concentration. Chemosphere 285, 131437.
- Easlon, H.M., Bloom, A.J., 2014. Easy Leaf Area: automated digital image analysis for rapid and accurate measurement of leaf area. Appl. Plant Sci. 2, 1400033.
- Ebrahimian, F., Lovato, G., Alvarado-Morales, M., Ashraf, M.T., Rodrigues, J.A.D., Tsapekos, P., et al., 2023. Iron limitation effect on H2/CO2 biomethanation: experimental and model analysis. J. Environ. Chem. Eng. 11.
- experimental and model analysis. J. Environ. Chem. Eng. 11.
 Fischer, A.M., Van Hamme, J.D., Gardner, W.C., Fraser, L.H., 2022. Impacts from topsoil stockpile height on soil geochemical properties in two mining operations in British Columbia: implications for restoration practices. Mining 2, 315–329.

- Freches, A., Fradinho, J.C., 2024. The biotechnological potential of the Chloroflexota phylum. Appl. Environ. Microbiol. 90, e0175623.
- Godinho, O., Devos, D.P., Quinteira, S., Lage, O.M., 2024. The influence of the phylum Planctomycetota in the environmental resistome. Res. Microbiol. 175, 104196.
- Gundale, M., Kardol, P., 2021. Multi-dimensionality as a path forward in plant-soil feedback research. J. Ecol. 109, 3446–3465.
- Harris, J.A., Birch, P., Short, K.C., 1993. The impact of storage of soils during opencast mining on the microbial community: a strategist theory interpretation. Restor. Ecol. 1, 88–100.
- Hernandez, J.A.C., Ribeiro, H.M., Bayne, E., MacKenzie, M.D., Lanoil, B.D., 2024. Impact of stockpile depth and storage time on soil microbial communities. Appl. Soil Ecol. 196
- Karnachuk, O.V., Panova, I.A., Rusanov, I.I., Schetinina, L., Lepokurova, O.Y., Domrocheva, E.V., et al., 2023. Coexistence of psychrophilic, mesophilic, and thermophilic sulfate-reducing Bacteria in a deep subsurface aquifer associated with coal-bed methane production. Microb. Ecol. 86, 1934–1946.
- Ledesma, J., Neilson, J.W., Maier, R.M., Babst-Kostecka, A., Rasmussen, C., 2025. Effects of stockpiling on topsoil biogeochemistry for semiarid mine reclamation. Min. Metall. Explor. 42, 15–26.
- Li, T., Wu, M., Duan, C., Li, S., Liu, C., 2022. The effect of different restoration approaches on vegetation development in metal mines. Sci. Total Environ. 806, 150626.
- Louca, S., Parfrey, L.W., Doebeli, M., 2016. Decoupling function and taxonomy in the global ocean microbiome. Science 353, 1272–1277.
- Madigan, M.T., Schaaf, N.A.V., Sattley, W.M., 2017. The Chlorobiaceae, Chloroflexaceae, and Heliobacteriaceae. In: Modern Topics in the Phototrophic Prokaryotes, pp. 139–161.
- Manero, A., Kragt, M., Standish, R., Miller, B., Jasper, D., Boggs, G., et al., 2020.
 A framework for developing completion criteria for mine closure and rehabilitation.
 J. Environ. Manag. 273, 111078.
- Mendez, M.O., Glenn, E.P., Maier, R.M., 2007. Phytostabilization potential of quailbush for mine tailings: growth, metal accumulation, and microbial community changes. J. Environ. Qual. 36, 245–253.
- Mleczek, M., Kozlowska, M., Kaczmarek, Z., Chadzinikolau, T., Golinski, P., 2012. Influence of Ca/Mg ratio on phytoextraction properties of Salix viminalis I. The effectiveness of Cd, Cu, Pb, and Zn bioaccumulation and plant growth. Int. J. Phytoremediation 14, 75–88.
- Murawska-Wlodarczyk, K., van der Ent, A., Wlodarczyk, T., Slomka, A., Paterson, D.J., Brueckner, D., et al., 2024. Habitat-specific allocations of elements in Atriplex lentiformis seeds hint at adaptation to metal toxicity. J. Exp. Bot. 75, 5076–5090.
- Mushia, N., Ramoelo, A., Ayisi, K., 2016. The impact of the quality of coal mine stockpile soils on sustainable vegetation growth and productivity. Sustainability 8.
- Nguyen, N.H., Song, Z., Bates, S.T., Branco, S., Tedersoo, L., Menke, J., et al., 2016. FUNGuild: an open annotation tool for parsing fungal community datasets by ecological guild. Fungal Ecol. 20, 241–248.
- Ogawa, M., Hanada, A., Yamauchi, Y., Kuwahara, A., Kamiya, Y., Yamaguchi, S., 2003. Gibberellin biosynthesis and response during Arabidopsis seed germination. Plant Cell 15, 1591–1604.
- Oksanen, J., Kindt, R., Legendre, P., O'Hara, B., Simpson, G.L., Solymos, P., et al., 2008. The vegan Package. Community Ecology Package, vol. 10, pp. 631–637.
- Palmer, J.S., Hough, R.L., West, H.M., Avery, L.M., 2019. A review of the abundance, behaviour and detection of clostridial pathogens in agricultural soils. Eur. J. Soil Sci. 70, 911–929.
- Pan, F., Yang, N., Zhu, X., Yu, C., Jiang, M., Jiang, Y., et al., 2023. Discovery of a natural hybrid polyketide produced by endophytic Cladosporium sphaerospermum for biocontrol of phytopathogenic fungus Botrytis cinerea. J. Agric. Food Chem. 71, 12190–12202.
- Peterson, R.A., Cavanaugh, J.E., 2019. Ordered quantile normalization: a semiparametric transformation built for the cross-validation era. J. Appl. Stat. 1–16 (0. Taylor & Francis).
- Petriglieri, F., Nierychlo, M., Nielsen, P.H., McIlroy, S.J., 2018. In situ visualisation of the abundant Chloroflexi populations in full-scale anaerobic digesters and the fate of immigrating species. PLoS One 13, e0206255.
- Randelovic, D., Jakovljevic, K., Sinzar-Sekulic, J., Kuzmic, F., Silc, U., 2024. Recognising the role of ruderal species in restoration of degraded lands. Sci. Total Environ. 938, 173104.
- Rungjindamai, N., Jones, E.B.G., 2024. Why are there so few Basidiomycota and basal fungi as endophytes? A review. J. Fungi (Basel) 10.
- Sarula, Hengshan Y., Ruifu, Z., Yuanyuan, L., 2023. Shallow-buried drip irrigation promoted the enrichment of beneficial microorganisms in surface soil. Rhizosphere 28.
- Schneider, C.A., Rasband, W.S., Eliceiri, K.W., 2012. NIH Image to ImageJ: 25 years of image analysis. Nat. Methods 9, 671–675.
- Shackelford, N., Paterno, G.B., Winkler, D.E., Erickson, T.E., Leger, E.A., Svejcar, L.N., et al., 2021. Drivers of seedling establishment success in dryland restoration efforts. Nat. Ecol. Evol. 5, 1283–1290.
- Soria, R., Ortega, R., Valiente, N., Rodriguez-Berbel, N., Lucas-Borja, M.E., Miralles, I., 2024. Monitoring of indicators and bacterial succession in organic-amended technosols for the restoration of semiarid ecosystems. Sci. Total Environ. 954, 176302.
- Spring, S., Rosenzweig, F., 2006. The genera Desulfitobacterium and Desulfosporosinus: taxonomy. In: The Prokaryotes, pp. 771–786.
- Taffner, J., Erlacher, A., Bragina, A., Berg, C., Moissl-Eichinger, C., Berg, G., 2018. What is the role of archaea in plants? New insights from the vegetation of Alpine bogs. mSphere 3.

- Takagi, D., Ishiyama, K., Suganami, M., Ushijima, T., Fujii, T., Tazoe, Y., et al., 2021.
 Manganese toxicity disrupts indole acetic acid homeostasis and suppresses the CO(2) assimilation reaction in rice leaves. Sci. Rep. 11, 20922.
- Thakur, M.P., van der Putten, W.H., Wilschut, R.A., Veen, G.F.C., Kardol, P., van Ruijven, J., et al., 2021. Plant-soil feedbacks and temporal dynamics of plant diversity-productivity relationships. Trends Ecol. Evol. 36, 651–661.
- van der Heyde, M., Bunce, M., Dixon, K., Wardell-Johnson, G., White, N.E., Nevill, P., 2020. Changes in soil microbial communities in post mine ecological restoration: implications for monitoring using high throughput DNA sequencing. Sci. Total Environ. 749, 142262.
- Walters, W., Hyde, E.R., Berg-Lyons, D., Ackermann, G., Humphrey, G., Parada, A., et al., 2016. Improved bacterial 16S rRNA gene (V4 and V4-5) and fungal internal transcribed spacer marker gene primers for microbial community surveys. mSystems 1, e00009-15.
- Weber, K.A., Achenbach, L.A., Coates, J.D., 2006. Microorganisms pumping iron: anaerobic microbial iron oxidation and reduction. Nat. Rev. Microbiol. 4, 752–764.
- Yamada, T., Sekiguchi, Y., Hanada, S., Imachi, H., Ohashi, A., Harada, H., et al., 2006. Anaerolinea thermolimosa sp. nov., Levilinea saccharolytica gen. nov., sp. nov. and Leptolinea tardivitalis gen. nov., sp. nov., novel filamentous anaerobes, and description of the new classes Anaerolineae classis nov. and Caldilineae classis nov. in the bacterial phylum Chloroflexi. Int. J. Syst. Evol. Microbiol. 56, 1331–1340.
- Zhao, X., Zheng, G.W., Niu, X.M., Li, W.Q., Wang, F.S., Li, S.H., 2009. Terpenes from Eupatorium adenophorum and their allelopathic effects on Arabidopsis seeds germination (dagger). J. Agric. Food Chem. 57, 478–482.
- Zheng, Y., Wang, H., Liu, Y., Zhu, B., Li, J., Yang, Y., et al., 2020. Methane-dependent mineral reduction by aerobic methanotrophs under hypoxia. Environ. Sci. Technol. Lett. 7, 606–612.
- Zhu, S.C., Zheng, H.X., Liu, W.S., Liu, C., Guo, M.N., Huot, H., et al., 2021. Plant-soil feedbacks for the restoration of degraded mine lands: a review. Front. Microbiol. 12, 751704